DOI:
10.1177/0003702819898275

Document Version
Peer reviewed version

Transmission Fourier Transform Infrared (FT-IR) Imaging, Mapping and Synchrotron Scanning Microscopy with ZnS Hemispheres on Living Mammalian Cells at Sub-Cellular Resolution

K. L. Andrew Chan[1]*, Ali Altharawi[1], Pedro Fale[2], Cai Li Song[3], Sergei G. Kazarian[3], Gianfelice Cinque[4], Valérie Untereiner[5,6] and Ganesh D Sockalingum[6]

[1]Institute of Pharmaceutical Science, School of Cancer and Pharmaceutical sciences, King's College London, SE1 9NH, UK

[2] University of Lisboa, Faculty of Sciences, BioISI - Biosystems & Integrative Sciences Institute, Lisboa, Portugal

[3]Department of Chemical Engineering, Imperial College London, South Kensington Campus, SW7 2AZ, UK

[4]Diamond Light Source, Harwell Science and Innovation Campus, Didcot, OX11 0DE, UK

[5]Plateforme en Imagerie Cellulaire et Tissulaire (PICT), University of Reims Champagne-Ardenne, Reims ? France

[6]University of Reims Champagne-Ardenne, BioSpecT EA7506, UFR Pharmacie, F-51096 Reims, France

Keywords: FT-IR imaging; Live cell; subcellular; nucleus; Lipid; label-free; ZnS hemispheres spatial resolution

Abstract

FTIR spectroscopic imaging and microscopy of single living cells are established label-free technique for the study of cell biology. The constant driver to improve the spatial resolution of the technique is due to the diffraction limit given by IR wavelength making subcellular study challenging. Recently we have reported, with the use of a prototype ZnS transmission cell made of two hemispheres, that the spatial resolution is improved by the factor of the refractive index of ZnS, achieving a $\lambda/2.7$ spatial resolution using the synchrotron-IR microscopy with a 36x objective with numerical aperture (NA) of 0.5.[1] To refine and to demonstrate that the ZnS hemisphere transmission device can be translated to standard bench-top FTIR imaging systems, we have, in this work, modified the device to achieve a more precise path length, which has improved the spectral quality of the living cells, and showed for the first time that the device can be applied to study live cells with three different bench-top FTIR imaging systems. We applied focal plane array (FPA) imaging, linear array and synchrotron single point scanning method and demonstrated that in all cases, subcellular details of individual living cells can be obtained. Results have shown that imaging with the FPA detector can measure the largest area in a given time whilst measurements from the scanning methods produced a smoother image. Synchrotron single point mapping produced the best quality image and has the flexibility to introduce over sampling to produce images of cells with great details, but it is time consuming in scanning mode. In summary, this work has demonstrated that the ZnS hemispheres can be applied in

all three spectroscopic approaches to improve the spatial resolution without any modification to the existing microscopes.

Introduction

FTIR imaging of live cells has been shown to be a promising tool for cell biology studies.[2-11] However, with the relatively long wavelength of infrared light especially in the so-called fingerprint region, the spatial resolution obtained is usually limited to approximately 3-30 μm with a standard FTIR imaging microscope, depending on the numerical aperture (NA) of the objective and the wavelength of light used to generate the FTIR image.[12, 13] This limits the study to the analysis of single cells for most mammalian cells, which have sizes in the 10-50 μm range, with subcellular features of a few micrometers and below, resulting in unresolved subcellular information.

There have been previous works to improve the spatial resolution in order to obtain subcellular features within a living cell. This includes the use of a synchrotron source to image[14, 15] or to map with aperture size reduced to just a few micrometre,[16] the use of high magnification and high NA objectives,[17] or to significantly increase the numerical aperture (NA) by using solid immersion approach such as micro-attenuated total reflection (ATR) objective and infrared transparent hemispheres.[3, 18-20] Using synchrotron source or high magnification objectives allow one to achieve diffraction limited images more easily but ultimately, the NA has to be increased to improve the diffraction limit. High NA objectives, e.g. NA of 0.62 and 0.8,[21] or solid immersion system to increase the NA a factor that is equivalent to the refractive index of the solid immersion element are used for this purpose. Recently, micro-ATR imaging has been shown to be able to resolve subcellular features including dried parasite infected red blood cells.[22] However, with the micro-ATR approach, the absorbance from the cell will be lower than when measured in transmission, and the evanescent wave might not probe the full thickness of the attached cell.[23] The higher the refractive index, the shallower the depth of penetration and the shorter the pathlength (a smaller absorbance), therefore the gain in spatial resolution is compromised by a lowering of the signal to noise ratio. Recently, it has been found that Ge is susceptible to erosion by the attached cell and would require a protective layer for cells attached for longer than a day.[24]

Another solid immersion approach that has shown to be applicable for live cell imaging in transmission is the use of two CaF_2 pseudo hemispheres to sandwich the live cells between a thin gap.[20] This approach was originally developed to remove dispersion from thick IR windows that are commonly used in transmission liquid cells. However, it was found that the pseudo-hemisphere approach with CaF_2 lenses also functioned as a solid immersion lens, which increased both the magnification and the spatial resolution of the image.[25] It was also demonstrated that this correcting lens approach forming two pseudo-hemispheres can be beneficially used for FTIR imaging of biological tissues and biomaterials.[23, 26, 27] The approach of pseudo-hemispheres led to further developments based on whole ZnS hemispheres. We later demonstrated that the ZnS hemispheres can also be used for the enhancement of spatial resolution and magnification in a Synchrotron-based IR mapping measurement. United Stated Air Force resolution target feature of 2.19 μm could be resolved at wavelength of 6 μm.[1] Zinc sulphide has the advantage of having a much lower spectral cut-off value of ~700 cm^{-1} than CaF_2, which has a cut-off value of ~1000 cm^{-1}, therefore it does not increase the noise level below ~1100 cm^{-1} region as in the case when CaF_2 is used. This is particularly beneficial for the linear array and single point mapping systems where the detectors

sensitivity range can reach down to 720 cm^{-1} and 650 cm^{-1}, respectively. Zinc sulphide also has a high refractive index of 2.25, which can produce a 225% enhancement in spatial resolution in transmission mode. It is also found to be compatible with many cell lines growth.[28] Our previous attempt was based on a prototype device which has little control over the pressure that holds the two hemispherical lenses together resulting in a relatively large path length through the transmission cell.[1] Recently, a new water correction method has been developed showing that high quality cell spectra can be obtained at 12 μm path length, which is thought to be less stressful for the cells than when a smaller path length is used, but would require the high brilliance of a synchrotron source.[29] In this work, we have improved the design of the transmission liquid cell where the two hemispherical lenses are held together tightly by means of a screw ring with a thin spacer of 6 micrometres Mylar film for a better throughput of light (Figure 1). The new design allows the path length through the liquid cell to be better controlled, whether it is 12 or 6 μm. This, thus improves the reproducibility and the signal-to-noise ratio of the measured spectra, which made it highly suitable for imaging using bench-top instruments with a Globar source. Secondly, we have extended the application of ZnS hemisphere transmission cell to FPA imaging and linear array imaging systems for the first time, which significantly reduces the imaging time. In this study, we present the novel findings that the ZnS hemisphere transmission device can be translated to different types of imaging systems whilst keeping its resolution enhancement effect. It is important to highlight that this work is based on transmission spectroscopy, which is distinguished from the previous works on ATR.[18, 19, 30]

Methods

Live cell culturing and preparations for FTIR spectroscopic measurements

Lung carcinoma A549 cells (**86012804** Sigma) were used as a model for live cell imaging. Cells were grown as described in our previous work.[1] In brief, cells were maintained in DMEM supplemented with 10% foetal bovine serum (FBS), 2mM L-glutamine and 100 unit mL^{-1} penicillin streptomycin at 37^{o}C in a 5% CO_2 incubator. Cells were harvested at ~80% confluency and sub-cultured on the flat surface of the ZnS hemisphere for 24 hours for attachment. Once cells were attached, the medium was replaced with L15 medium, supplemented with 10% FBS, 2mM L-glutamine and 100 unit mL^{-1} of penicillin streptomycin. The ZnS hemisphere with the attached cells was carefully mounted onto a lens holder (Thorlabs Inc., New Jersey, US) with in-house made lens mount adaptor (Figure 1a), where the cells were sandwiched between two ZnS hemispheres with a new 6-μm spacer prepared by in house surgical razor-cut 6-μm thick Mylar® film (VHG LABS, LGC Standards, USA). In all experiments, once the hemispheres were aligned in the microscope, a background was taken from an area near the centre of the hemisphere that is not occupied by cells. The medium used contains mostly water with only 0.3 wt% amino acids, 0.4 wt% protein, 0.02 wt% phosphate and 0.1 wt% carbohydrates, i.e. the compounds that may interfere with the spectrum are at a much lower concentration than in the living cell.

(a)

(b)

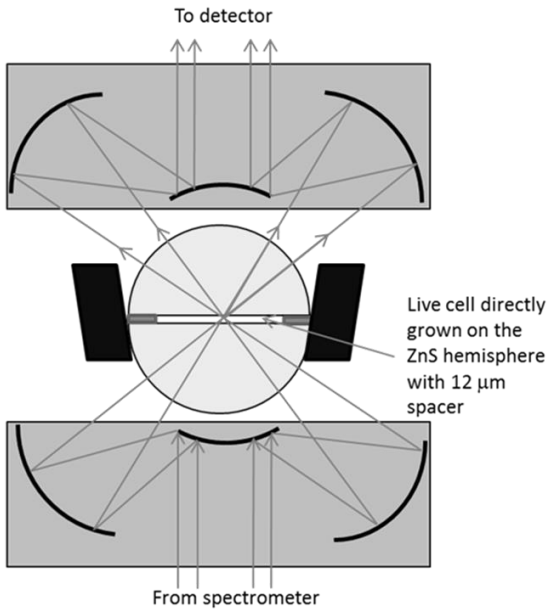

(c)

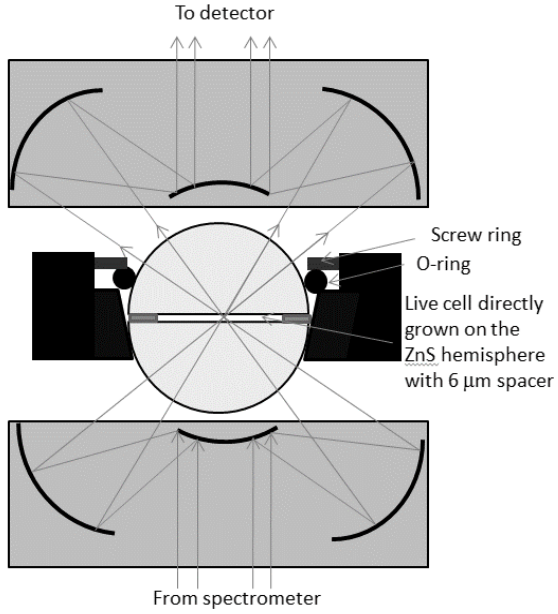

Figure 1: (a) A photograph of the new transmission device (in vertical position) with two ZnS hemispheres held in a lens holder. The bottom schematics show the beam path through the ZnS hemisphere in horizontal position in (b) the old design[1] and (c) the new design used in this study.

Synchrotron FTIR microscopy

Experiments were carried out at the Diamond Light Source synchrotron facility, specifically the B22 beamline *MIRIAM*. FTIR imaging microscope system (Hyperion 3000, Bruker Optics) containing a 36x reverse Cassegrain reflective objective (NA=0.5 in air, increases to 1.13 through the ZnS hemisphere

- note that all NA and spatial resolution values through the ZnS hemisphere are calculated based on the refractive index of ZnS at 2.25, which is an estimate and the maximum NA through the ZnS hemisphere is ~1.3 for higher NA will results in internal reflection. The actual value may vary due to the dispersion effect and uncertainty in the refractive index of cells), a matching condenser and a mid-band mercury cadmium telluride (MCT) single element detector with a 50 μm pitch size and a cut-off wavelength at *ca*. 650cm^{-1} was used. A multilayer Ge filter (Bruker Optics) was used to reduce the spectral range below 4000 cm^{-1} of the incoming beam, and the non-linearity of the detector was corrected with the spectrometer software during acquisition.

FTIR images of cells between the two ZnS hemispheres were then captured by mapping with a 6 μm x 6 μm aperture (i.e. 2.7 μm x 2.7 μm after magnification through the ZnS hemisphere) with a nominal step size of 2 μm (i.e., 0.89 μm through the ZnS hemisphere). Measurements were obtained immediately after assembling the transmission device by averaging 128 scans at 4 cm^{-1} spectral resolution giving a scanning time of 20 seconds per spectrum. A background with 256 scans was measured in an area that is clear of cells, which takes 40 seconds. Cells remain viable in the transmission device for more than 12 hours as was confirmed in our previous study.[1]

FTIR spectroscopic imaging with FPA detector

Experiments were carried out using both Bruker FTIR imaging microscope system (Hyperion 3000, Bruker Optics) equipped with a 64 x 64 FPA detector and a 15x objective (NA=0.4, increases to ~0.9 through the ZnS hemisphere) and an Agilent FTIR imaging microscope with the normal magnification mode (15x objective, NA=0.62, increases to a maximum of ~1.3 through the ZnS hemisphere).[31]

The FPA FTIR imaging system with the Bruker microscope has a pixel size of 2.67 μm. Magnification through the ZnS hemispheres yields a smaller projected pixel size of ~1.2 μm. Pixel binning of 2x2 was applied to the FTIR image obtained, therefore the final pixel size of the image (shown in this paper) is ~2.4 μm. On the other hand, the FPA FTIR imaging with the Agilent microscope produces a pixel size of 5.5 μm through the 15x objective, (i.e. an approximate 2x reduction from the microscope objective to the FPA detector). Through the ZnS hemispheres, the calculated pixel size was reduced to ~2.4 μm. The measurement was made with 512 scans at 4 cm^{-1} spectral resolution (~20 min acquisition time per image, a total of 40 min including background measurement).

Linear array FTIR mapping

A Perkin Elmer Spotlight 400 in high-magnification mode (i.e., 6.25 μm per pixel, NA=0.6, increases to a maximum of ~1.3 through the ZnS hemisphere) was used for the linear array FTIR mapping. The calculated pixel size through the ZnS hemispheres was ~2.78 μm. The measurement was made with 128 scans per spectrum at 4 cm^{-1} spectral resolution (~45 min per image). A background is measured in a cell-free area with a similar number of scans, which took 6.5 min to measure.

Spectral image data analysis.

FTIR images were generated using the software provided by the instrument or external spectral analysis packages. The images collected from the Bruker imaging systems (for both FPA and synchrotron mapping) were processed using the OPUS 7.8 software. Images collected using the Perkin Elmer Spotlight 400 were processed using the SpectrumIMAGE software. Images collected

using the Agilent were processed using the ISys 2.1 software (Malven). In all cases, images were generated by integrating the area under the band within the same spectral range specified with a straight baseline drawn between the integral limits. Bands of protein amide II (range 1593-1496 cm^{-1}), $\nu_{sym}(PO_2)^-$ (range 1102-1065 cm^{-1}), lipid ν(C=O) (range 1763-1718 cm^{-1}), lipid (predominantly) $\nu(CH_2)$ (range 2946-2908 cm^{-1}) and DNA base ν(C=O) (range 1730-1707 cm^{-1}) were used to generate the images.

Results and discussions

FTIR images of live A549 cells measured using the FPA detectors, linear array detector and synchrotron mapping with a single element detector are shown in Figure 2 (Images are also available in grey scale in supplementary Figure S1). The measurement parameters were chosen such that each imaging method produced a similar spectral noise level. The images were adjusted to the same length scale and cropped to a similar size (apart from the smaller synchrotron mapping) such that a direct comparison between images can be made. The exact same cells were imaged for Figure 2b-k and 2m-v such that a comparison between different FPA and linear array detectors can be made. A cell of similar size and shape was imaged using the synchrotron mapping approach and the results are also shown in Figure 2.

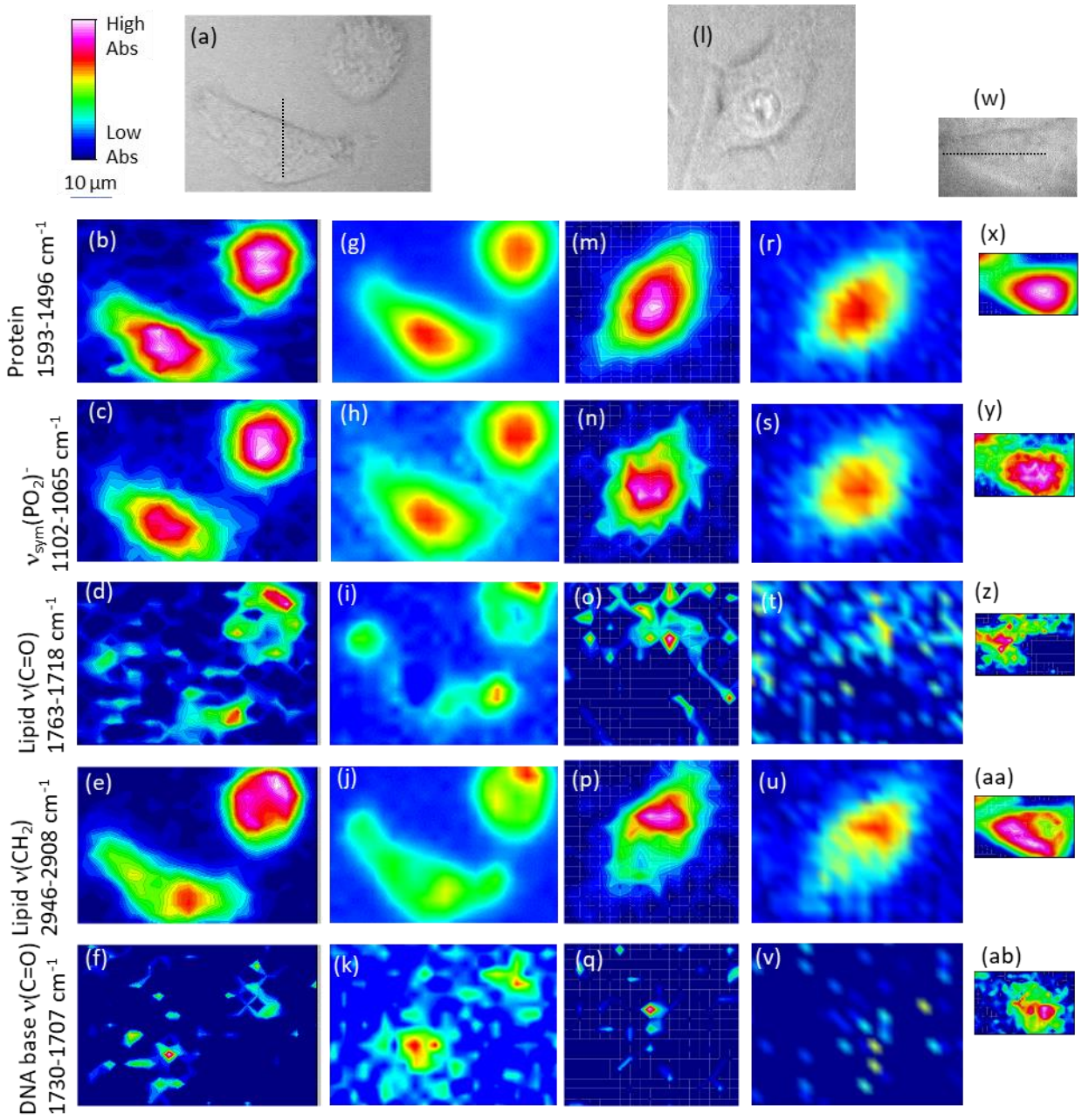

Figure 2: FTIR images of live A549 cells in the ZnS hemispheres transmission device measured with the Bruker FPA FTIR microscope (b-f and m-q), Agilent FPA FTIR microscope (r-v), the linear array FTIR microscope (g-k) and the MIRIAM synchrotron FTIR microscope (x-ab). The integration range used to generate the images are indicated on the left. (a), (l) and (w) shows the visible image of the cells for images (b-k), (m-v) and (x-ab), respectively. All images are adjusted to the same length scale and the scale bar is shown near the top left of the Figure. An enlarged version of image (w-ab) is included in supplementary Figure S2.

The results have clearly shown that the ZnS hemispheres transmission cell is applicable to all imaging systems tested and produced images of cells with subcellular details. For example, the FTIR images generated using the protein amide II peak has shown a clear and accurate outline of the cells when compared to the visible images. Images generated using the two lipid bands base on the ν_{asym}(C-H) mode (Figure 2e, j, p, u and aa) and the ν(C=O) mode at 1745 cm^{-1}, which has been assigned to the

ester band of the phospholipids, show remarkable differences and are different from the images generated using the protein amide II band. This is in good agreement with our previous observations[1] that not all lipid domains in a cell contains the same concentration of phospholipids, and high concentration of phospholipids expected in cell organelles such as Golgi apparatus and endoplasmic reticulum.[32, 33] Endoplasmic reticulum is a cell organelle that mainly comprises a network of membrane cisternae that are found surrounding the nucleus, and is continuous with the outer nuclear membrane.

Interestingly, the peak at 1714 cm^{-1}, which can be assigned to the nucleobase ν(C=O) in the double stranded DNA and is not easily observed in living cells,[34] is detectable and can be used to generate images of the distribution of DNA in cell (1730-1707 cm^{-1} in Figure 2f, k, q, v and ab). The thinner layer of water produced from the 6 µm spacer has helped to reduce the interference from the medium, allowing the relatively weak 1714 cm^{-1} band that is next to the nearby strong water absorbance to be observed. Spectra extracted from the outside nucleus and nucleus regions from Figure 2ab are shown in Figure 3 to highlight the small band at 1714 cm^{-1} is distinguishable from the lipid 1745 cm^{-1} band. Traditionally the band at 1087 cm^{-1} was used instead to map the nucleus of cells based on the $\nu_{sym}(PO_2)^-$ in the DNA backbone because it is a stronger band. However, using the band at 1714 cm^{-1} to map the distribution of the DNA is more specific than the 1087 cm^{-1} band as other non-nucleus specific biocomponents such as RNA, phospholipid, phosphorylated protein[35] and other phosphate containing metabolites such as adenosine triphosphate (ATP) and adenosine diphosphate (ADP) can contribute to the absorbance in that region. As a result, images generated from the integrated absorbance within the 1102–1065 cm^{-1} spectral range (Figure 2c, h, n, s and y) has shown a larger domain than the image generated using the 1730-1707 cm^{-1} range since RNA and other phosphate metabolites, which are not specific to the nucleus, also absorb in the 1087 cm^{-1} region. In fact, the images generated using the 1087 cm^{-1} band show a rather similar size and shape (of the distribution of the components corresponding to the spectral band) as the images generated for the amide II spectral band. In contrast, the images generated at 1714 cm^{-1} highlight a small area near the middle of the living cell where the nucleus is expected to be found.

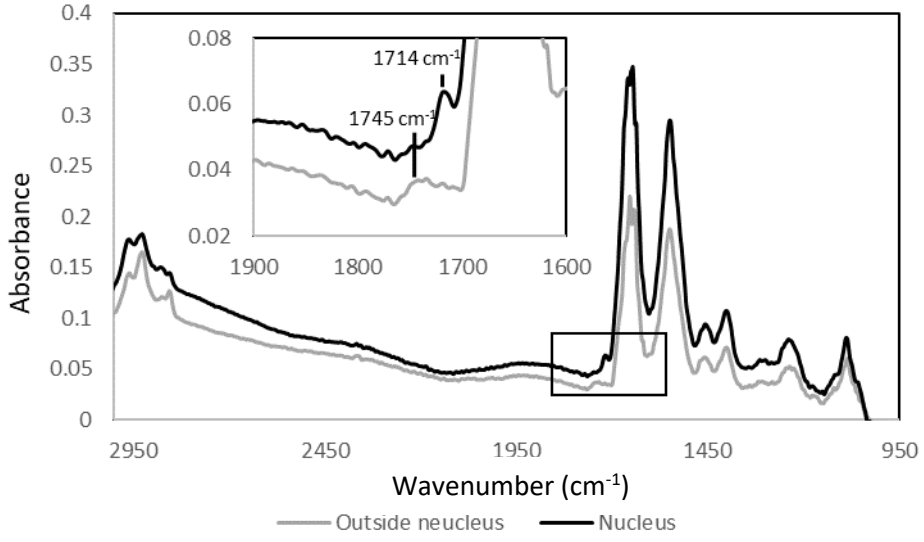

Figure 3: Spectra extracted from the nucleus and outside nucleus region of the cell shown in Figure 2ab. The insert shows the zoom-in spectra of the carbonyl spectral region.

The synchrotron map was obtained by a 3-fold oversampling approach, with the sacrifice of a 9-fold increase in measurement time, such that the pixel density is 3x higher that the other imaging approach to produce smoother images. The confocal effect from the aperture should also improve the sharpness of the image.[36] In particular, the image obtained using the synchrotron system (Figure 2ab) has shown well defined images with a clear round outline of the nucleus, which is different to the overall triangular shape of the cell as shown by the visible image in Figure 2w. Figure 2ab also shows some substructures of the nucleus where small spots of ~5 μm in diameter of high DNA concentrations are detected. These high density DNA regions may correspond to regions of tightly packed DNA in heterochromatin.

A direct comparison between the synchrotron imaging system with others, however, is not possible in this study because the living cells will change when left for more than a few hours and therefore different cells were measured in the other imaging systems. On the other hand, comparisons can be made between Figure 2b-k and m-v because they are the same cell and the time difference between the measurements was less than an hour, where minimal changes in to the cell is expected. Comparing Figures 2f and 2k, the former has shown some small spots of high integral values around the nucleus region but the image of the nucleus was not clear. Figure 2k, on the other hand, has shown a clear domain of the nucleus, similar to Figure 2ab. Although the Bruker FPA systems have a smaller projected pixel size, the FTIR image of the DNA base is less clear. In fact, the image of the nucleus before pixel binning is worse (see supplementary Figure S3). Spectra extracted across the cell from the two systems are shown in Figure 4.

Figure 2m-q and 2r-v show that both Bruker and Agilent FPA systems capture similar images of the cell but without a clear domain of the nucleus despite Figure 2l has clearly shown a nucleus of around 10 μm in diameter. One of the potential explanations for the lower image quality from the DNA base band is that individual spectrum measured by the FPA systems are obtained from different detector elements in the FPA. The difference in sensitivity and noises between pixels, which is a characteristic of the FPA, could affect the image quality. It also appears that the effect of atmospheric water vapour on the spectrum tends to have small variations between pixels for the FPA system as shown in Figure 4a. Pixel binning, apart from reducing the spectral noise, can also smooth out the pixel-to-pixel variation as shown in the Figure S3. In contrast, the pixel to pixel variations in the images obtained by scanning from the synchrotron and linear array system are less significant resulting in reduced image noise. It is important to note that the pixel-to-pixel noise affects images that are generated using smaller spectral bands such as the lipid ν(C=O) band and the DNA base ν(C=O) bands, where small changes in atmospheric water vapour peaks could have a significant impact, but not as significant for stronger bands such as the amide II. Furthermore, the FPA images shown in Figure 2 were cropped to focus on the area where the cells were located. The original imaged areas were ~2-fold and 4-fold larger for the Bruker and the Agilent systems, respectively. That means for the same length of imaging time, the FPA systems can analyse images of more cells than the scanning approaches. While this could be an advantage, the larger area could introduce difficulties in obtaining a good background from a cell free region, especially when cells are highly confluent.

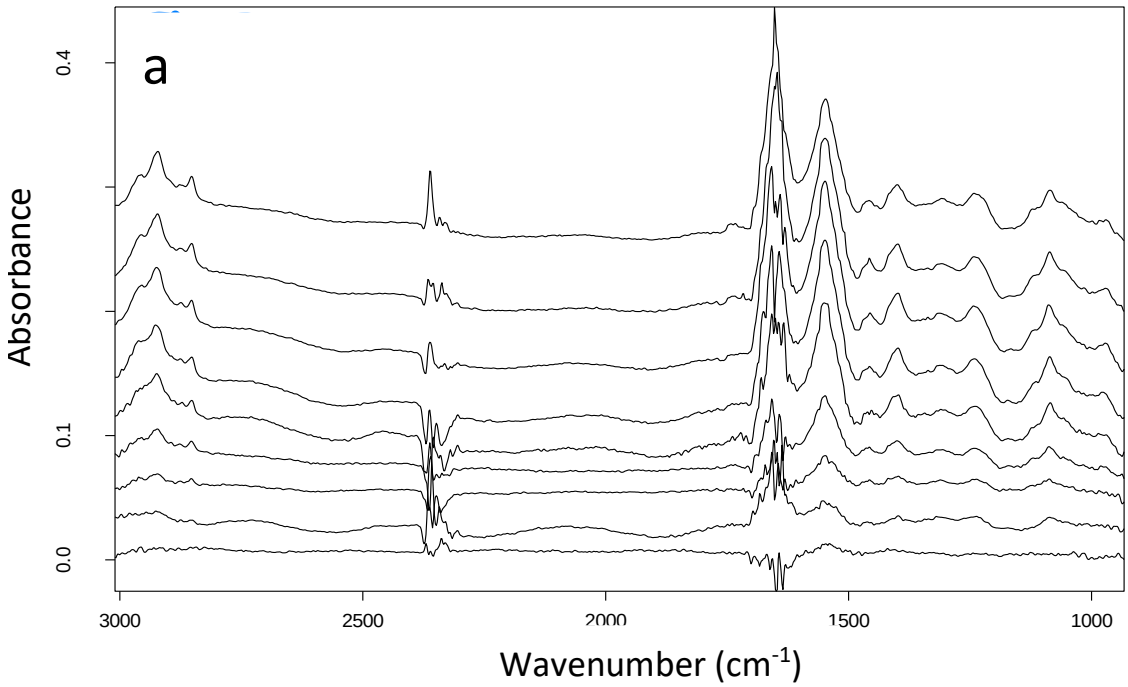
a
Absorbance
0.4
0.1
0.0
3000
2500
2000
1500
1000
Wavenumber (cm-1)

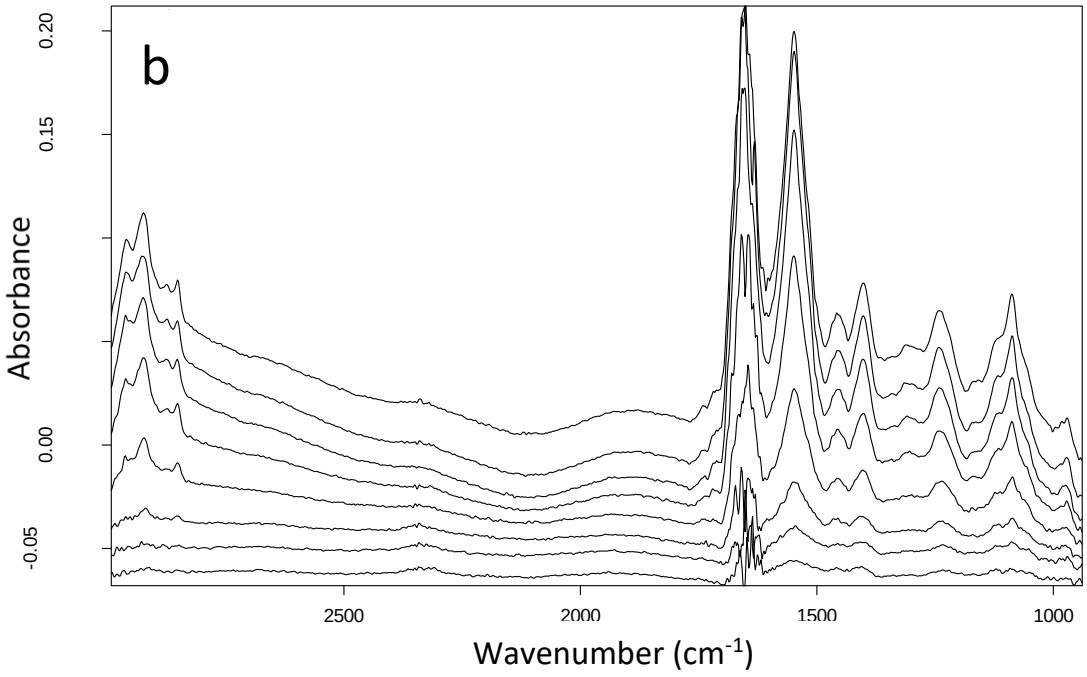
b
Absorbance
0.20
0.15
0.00
-0.05
2500
2000
1500
1000
Wavenumber (cm-1)

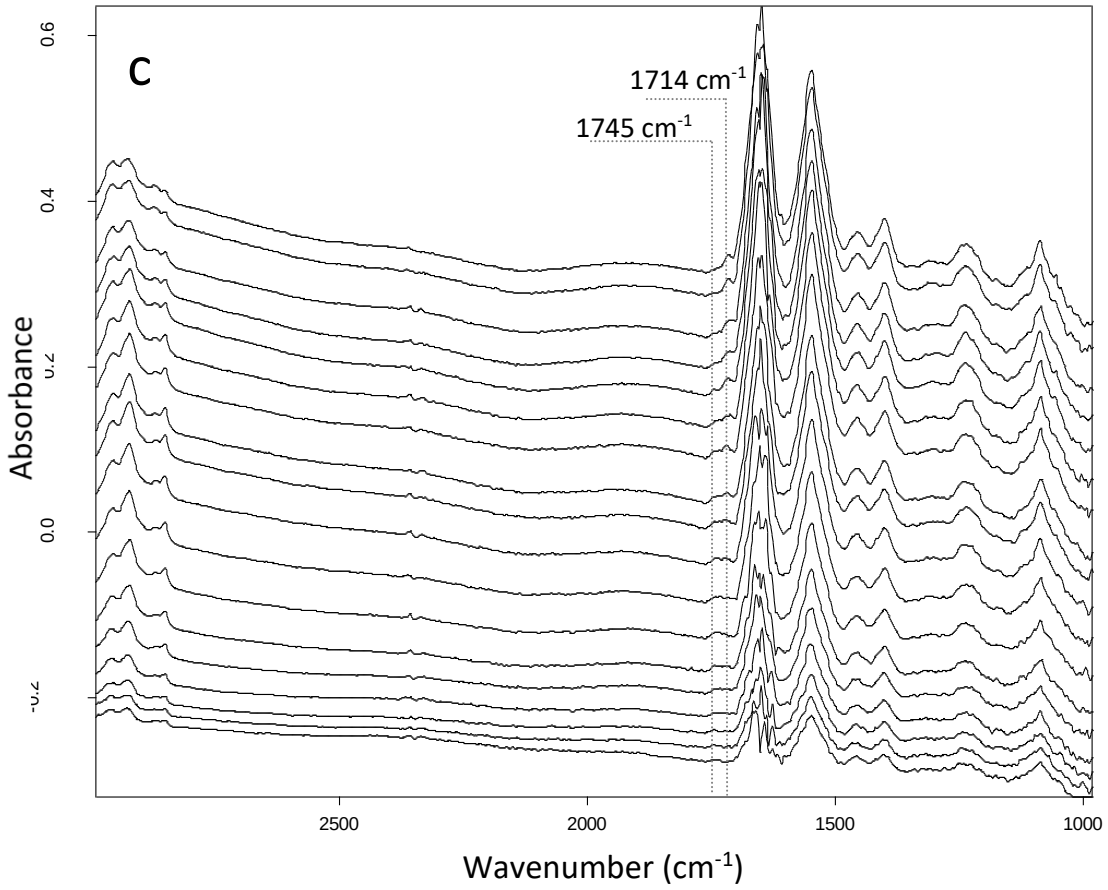

Figure 4: Representative spectra (unprocessed) extracted along a line (shown in Figure 2 a and w) from the edge (bottom spectrum) to the centre (top spectrum) of the live cell measured in the a) Bruker FPA b) Perkin Elmer linear array and c) Bruker synchrotron mapping system through the new ZnS hemisphere device. Spectra were shifted up or down along the Y-axis for a better presentation.

Spectra extracted across the living cell (indicated in Figure 2a and w) are shown in Figure 4 demonstrating the high quality spectra obtained by this method. The spectral region where water δ(O-H) has strong IR absorbance (at ~1680-1620 cm^{-1}) has shown a higher noise in all imaging systems. However, this is a marked improvement compares to the prototype device used in the previous measurement. The quality of spectra has been improved in the amide I region and the reduction of fringes in the baseline (See supplementary Figure S4). Furthermore, an image measurement of pure water was also obtained through the hemisphere transmission device and the result has shown that the integrated absorbance value between 1750-1480 cm^{-1} with a straight baseline between the integral limits varied marginally between 0.46 and 0.47 across the imaged area. This has demonstrated the pathlength in the transmission device is uniform (see Figure 5). Figure 4 has shown that high SNR (~150 for the amide II band against the peak to peak noise at 2000 cm^{-1}) are achieved in all imaging systems. The high spectral quality obtained with synchrotron micro FTIR is exemplified by the small but clear absorption band just above 1700cm^{-1} which is well above the noise level and distinguishable with respect to the other spectra shown in Figure 4. Spectra from the synchrotron mapping results in Figure 4c has shown a clear transition from lipid-rich region near the edge of the cell to the DNA-rich region near the centre of the cell. A clear band at 1745 cm^{-1} is observed near the edge of the cell and a clear band at 1714 cm^{-1} is observed in the centre of the cell.

Spectra extracted from the linear array imaging results in Figure 4b has shown a similar trend, but the transition is less obvious while the FPA imaging results did not show this trend, supporting the observations made in Figure 2.

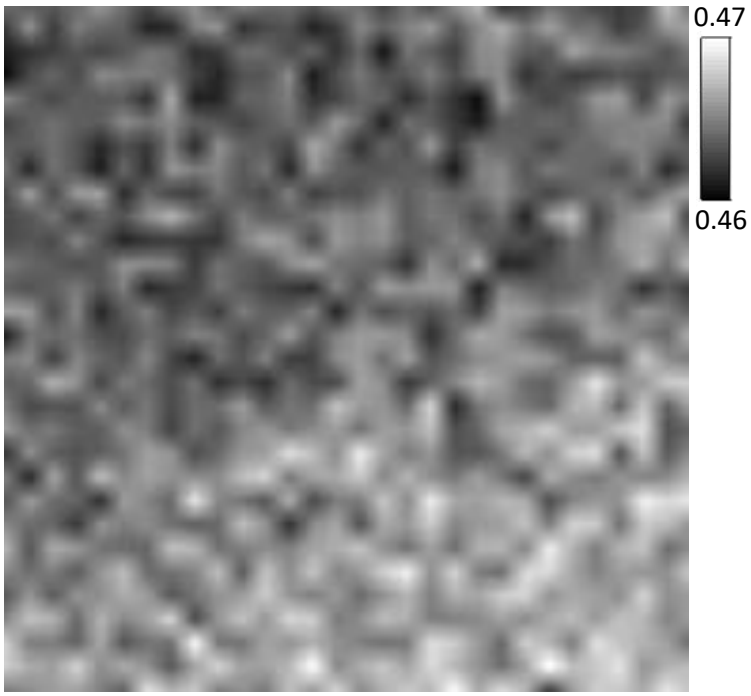

Figure 5: FTIR image of pure water based on the integration range of 1750-1480 cm^{-1} (imaging area of ~90 µm x 90 µm) through the ZnS hemisphere transmission device. A small range of value was used in the grey scale showing that the absorbance, hence the pathlength, of the transmission device is uniform.

Conclusions

We applied FTIR spectroscopic imaging with focal plane arrays (FPA), linear array and synchrotron single point mapping methods and demonstrated that in all cases, subcellular details of individual living cells can be obtained by using the ZnS hemispheres. Results have shown that the linear array and synchrotron mapping produced a smoother image than the FPA when weak bands are used to generate images due to the reduced pixel-to-pixel noise. Synchrotron mapping produced images of cells in great detail because of the higher pixel density from the 3-fold spatial oversampling and high spectral quality because of the confocal effect from the aperture which further sharpen the image, but it is also the slowest method out of the three tested approaches. In summary, the presented work has demonstrated that the ZnS hemispheres can be applied in all three imaging approaches to improve the spatial resolution without any modification to the existing microscope.

Supplementary Materials

Other underlying research materials related to this paper can be accessed by directly contacting the corresponding author.

Acknowledgements

We thank Diamond Light Source for access to the MIRIAM beamline under project N° SM17501 that contributed to the results presented here. We thank the Royal Society for the international exchanges grant (IE160964). We thank the Prince Sattam Bin Abdulaziz University for Ali Altharawi's PhD scholarship. We also thank BioISI for supporting the participation of Dr Fale through the UID/MULTI/04046/2019 Research Unit grant from FCT, Portugal (to BioISI). The Reims PICT Platform is gratefully acknowledged for instrument access.

The authors declare that there is no conflict of interest.

Reference

1. K. L. A. Chan, P. L. V. Fale, A. Atharawi, K. Wehbe, and G. Cinque. "Subcellular mapping of living cells via synchrotron microFTIR and ZnS hemispheres" Anal. Bioanal. Chem. 2018. 410(25): 6477-6487.
2. D. A. Moss, M. Keese, and R. Pepperkok. "IR micro spectroscopy of live cells" Vib. Spectrosc. 2005. 38(1-2): 185-191.
3. M. K. Kuimova, K. L. A. Chan, and S. G. Kazarian. "Chemical Imaging of Live Cancer Cells in the Natural Aqueous Environment" Appl. Spectrosc. 2009. 63(2): 164-171.
4. E. J. Marcsisin, C. M. Uttero, M. Miljkovic, and M. Diem. "Infrared microspectroscopy of live cells in aqueous media" Analyst. 2010. 135(12): 3227-3232.
5. K. L. Munro, K. R. Bambery, E. A. Carter, L. Puskar, M. J. Tobin, B. R. Wood, and C. T. Dillon. "Synchrotron radiation infrared microspectroscopy of arsenic-induced changes to intracellular biomolecules in live leukemia cells" Vib. Spectrosc. 2010. 53(1): 39-44.
6. L. Vaccari, G. Birarda, L. Businaro, S. Pacor, and G. Grenci. "Infrared Microspectroscopy of Live Cells in Microfluidic Devices (MD-IRMS): Toward a Powerful Label-Free Cell-Based Assay" Anal. Chem. 2012. 84(11): 4768-4775.
7. M. J. Baker, J. Trevisan, P. Bassan, R. Bhargava, H. J. Butler, K. M. Dorling, P. R. Fielden, S. W. Fogarty, N. J. Fullwood, K. A. Heys, C. Hughes, P. Lasch, P. L. Martin-Hirsch, B. Obinaju, G. D. Sockalingum, J. Sule-Suso, R. J. Strong, M. J. Walsh, B. R. Wood, P. Gardner, and F. L. Martin. "Using Fourier transform IR spectroscopy to analyze biological materials" Nature Protocols. 2014. 9(8): 1771-1791.
8. G. Clemens, J. R. Hands, K. M. Dorling, and M. J. Baker. "Vibrational spectroscopic methods for cytology and cellular research" Analyst. 2014. 139(18): 4411-4444.
9. J. Vongsvivut, P. Heraud, A. Gupta, T. Thyagarajan, M. Puri, D. McNaughton, and C. J. Barrow. "Synchrotron-FTIR Microspectroscopy Enables the Distinction of Lipid Accumulation in Thraustochytrid Strains Through Analysis of Individual Live Cells" Protist. 2015. 166(1): 106-121.
10. K. L. A. Chan and P. L. V. Fale. "Label-free optical imaging of live cells". In: I. Meglinski, editor. Biophotonics for medical applications. Woodhead Publishing, 2015. Vol. 1, Chap. 8, 215-241
11. J. Doherty, G. Cinque, and P. Gardner. "Single-cell analysis using Fourier transform infrared microspectroscopy" Appl. Spectrosc. Rev. 2017. 52(6): 560-587.
12. K. L. A. Chan, S. G. Kazarian, A. Mavraki, and D. R. Williams. "Fourier transform infrared imaging of human hair with a high spatial resolution without the use of a synchrotron " Appl. Spectrosc. 2005. 59(2): 149-155.
13. P. Lasch and D. Naumann. "Spatial resolution in infrared micro spectroscopic imaging of tissues" Biochim. Biophys. Acta-Biomembr. 2006. 1758(7): 814-829.
14. E. C. Mattson, E. Aboualizadeh, M. E. Barabas, C. L. Stucky, and C. J. Hirschmugl. "Opportunities for Live Cell FT-Infrared Imaging: Macromolecule Identification with 2D and 3D Localization" Int. J. of Mol. Sci. 2013. 14(11): 22753-22781.

15. S. W. Fogarty, Patel, II, J. Trevisan, T. Nakamura, C. J. Hirschmugl, N. J. Fullwood, and F. L. Martin. "Sub-cellular spectrochemical imaging of isolated human corneal cells employing synchrotron radiation-based Fourier-transform infrared microspectroscopy" Analyst. 2013. 138(1): 240-248.
16. C. Sandt, J. Frederick, and P. Dumas. "Profiling pluripotent stem cells and organelles using synchrotron radiation infrared microspectroscopy" J. Biophotonics. 2013. 6(1): 60-72.
17. P. Gelfand, R. J. Smith, E. Stavitski, D. R. Borchelt, and L. M. Miller. "Characterization of Protein Structural Changes in Living Cells Using Time-Lapsed FTIR Imaging" Anal. Chem. 2015. 87(12): 6025-6031.
18. Q. Wu, L. P. Ghislain, and V. B. Elings. "Imaging with solid immersion lenses, spatial resolution, and applications" Proceedings of the IEEE. 2000. 88(9): 1491-1498.
19. K. L. A. Chan and S. G. Kazarian. "New opportunities in micro- and macro-attenuated total reflection infrared spectroscopic imaging: Spatial resolution and sampling versatility" Appl. Spectrosc. 2003. 57(4): 381-389.
20. K. L. A. Chan and S. G. Kazarian. "Correcting the Effect of Refraction and Dispersion of Light in FT-IR Spectroscopic Imaging in Transmission through Thick Infrared Windows" Anal. Chem. 2013. 85(2): 1029-1036.
21. J. Nallala, G. R. Lloyd, M. Hermes, N. Shepherd, and N. Stone. "Enhanced spectral histology in the colon using high-magnification benchtop FTIR imaging" Vib. Spectrosc. 2017. 91(S1): 83-91.
22. J. Vongsvivut, P.-G. D, B. R. Wood, P. Heraud, K. Khambatta, D. Hartnell, M. J. Hackett, and M. J. Tobin. "Synchrotron macro ATR-FTIR microspectroscopy for high-resolution chemical mapping of single cells" Analyst. 2019. 144(10): 3226-3238.
23. A. Sroka-Bartnicka, J. A. Kimber, L. Borkowski, M. Pawlowska, I. Polkowska, G. Kalisz, A. Belcarz, K. Jozwiak, G. Ginalska, and S. G. Kazarian. "The biocompatibility of carbon hydroxyapatite/beta-glucan composite for bone tissue engineering studied with Raman and FTIR spectroscopic imaging" Anal. Bioanal. Chem. 2015. 407(25): 7775-7785.
24. P. L. V. Fale and K. L. A. Chan. "Preventing damage of germanium optical material in attenuated total reflection-Fourier transform infrared (ATR-FTIR) studies of living cells" Vib. Spectrosc. 2017. 91(S1): 59-67.
25. K. L. A. Chan and S. G. Kazarian. "Aberration-free FTIR spectroscopic imaging of live cells in microfluidic devices" Analyst. 2013. 138(14): 4040-4047.
26. J. A. Kimber, L. Foreman, B. Turner, P. Rich, and S. G. Kazarian. "FTIR spectroscopic imaging and mapping with correcting lenses for studies of biological cells and tissues" Faraday Discussions. 2016. 187: 69-85.
27. J. A. Kimber and S. G. Kazarian. "Spectroscopic imaging of biomaterials and biological systems with FTIR microscopy or with quantum cascade lasers" Anal. Bioanal. Chem. 2017. 409(25): 5813-5820.
28. K. Wehbe, J. Filik, M. D. Frogley, and G. Cinque. "The effect of optical substrates on micro-FTIR analysis of single mammalian cells" Anal. Bioanal. Chem. 2013. 405(4): 1311-1324.
29. J. Doherty, Z. Zhang, K. Wehbe, G. Cinque, P. Gardner, and J. Denbigh. "Increased optical pathlength through aqueous media for the infrared microanalysis of live cells" Anal. Bioanal. Chem. 2018. 410(23): 5779-5789.
30. B. M. Patterson, G. J. Havrilla, C. Marcott, and G. M. Story. "Infrared microspectroscopic imaging using a large radius germanium internal reflection element and a focal plane array detector" Appl. Spectrosc. 2007. 61(11): 1147-1152.
31. S. G. Kazarian and K. L. A. Chan. "Micro- and Macro-Attenuated Total Reflection Fourier Transform Infrared Spectroscopic Imaging" Appl. Spectrosc. 2010. 64(5): 135A-152A.
32. E. Gazi, J. Dwyer, N. P. Lockyer, J. Miyan, P. Gardner, C. A. Hart, M. D. Brown, and N. W. Clarke. "A study of cytokinetic and motile prostate cancer cells using synchrotron-based FTIR micro spectroscopic imaging" Vib. Spectrosc. 2005. 38(1-2): 193-201.

33. G. van Meer, D. R. Voelker, and G. W. Feigenson. "Membrane lipids: where they are and how they behave" Nature Reviews Molecular Cell Biology. 2008. 9(2): 112-124.
34. D. R. Whelan, K. R. Bambery, P. Heraud, M. J. Tobin, M. Diem, D. McNaughton, and B. R. Wood. "Monitoring the reversible B to A-like transition of DNA in eukaryotic cells using Fourier transform infrared spectroscopy" Nucleic Acids Res. 2011. 39(13): 5439-5448.
35. A. Altharawi, K. M. Rahman, and K. L. A. Chan. "Towards identifying the mode of action of drugs using live-cell FTIR spectroscopy" Analyst. 2019. 144(8): 2725-2735.
36. L. G. Carr, L. M. Miller, and P. Dumas. "Synchrotron radiation as a source for infrared microspectroscopic imaging with 2D multi-element detection". In: D. Moss, editor. Biomedical applications of synchrotron infrared microscopectroscopy. UK: RSC Publishing, 2011.Vol. 7,226-259

Supplementary

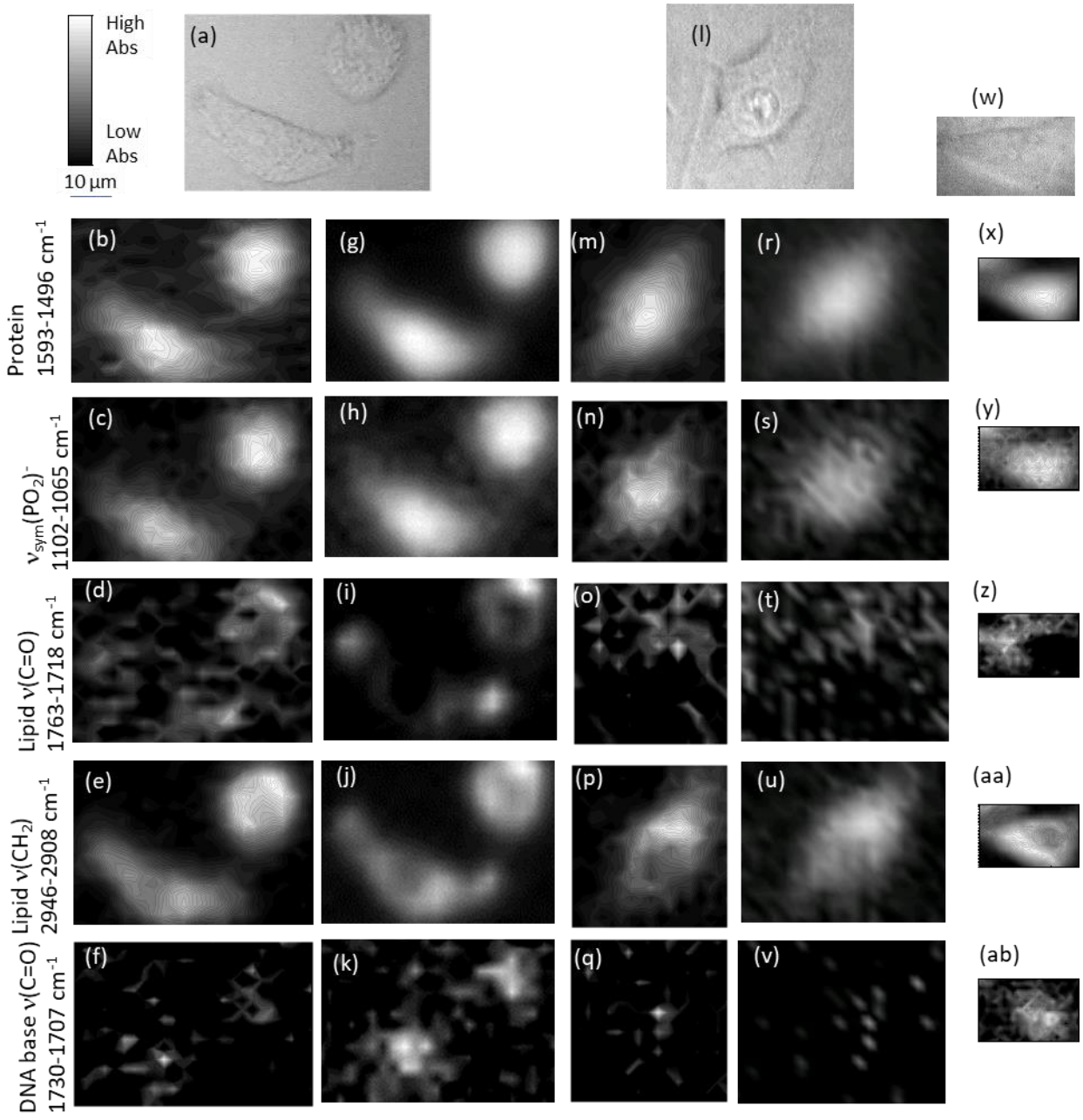

Figure S1: Grey scale version of Figure 2 in the main text.

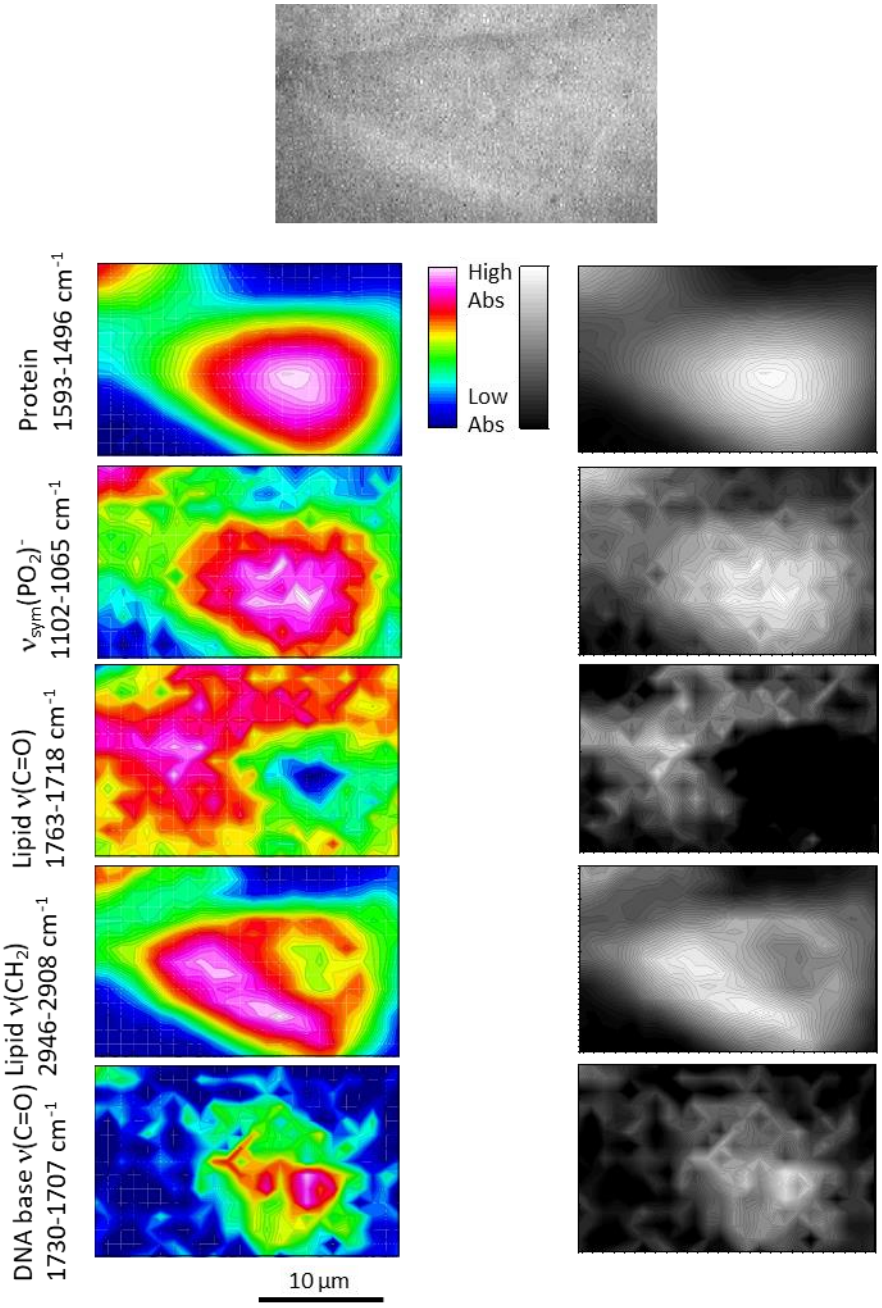

Figure S2: Enlarge version of images shown in Figure 2W-2AB in false colour map (left column) and in grey scale (right column).

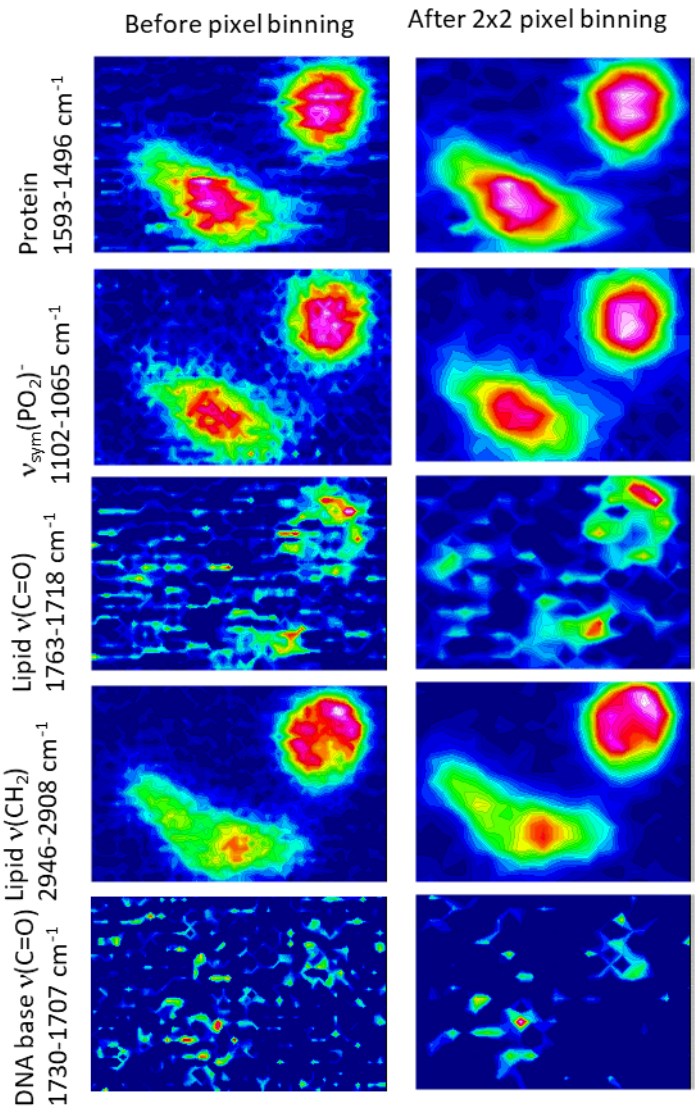

Figure S3: FTIR images of cells measured using the Bruker FPA imaging system (shown in Figure 2B-F in the main document) before (left column) and after (right column) pixel binning.

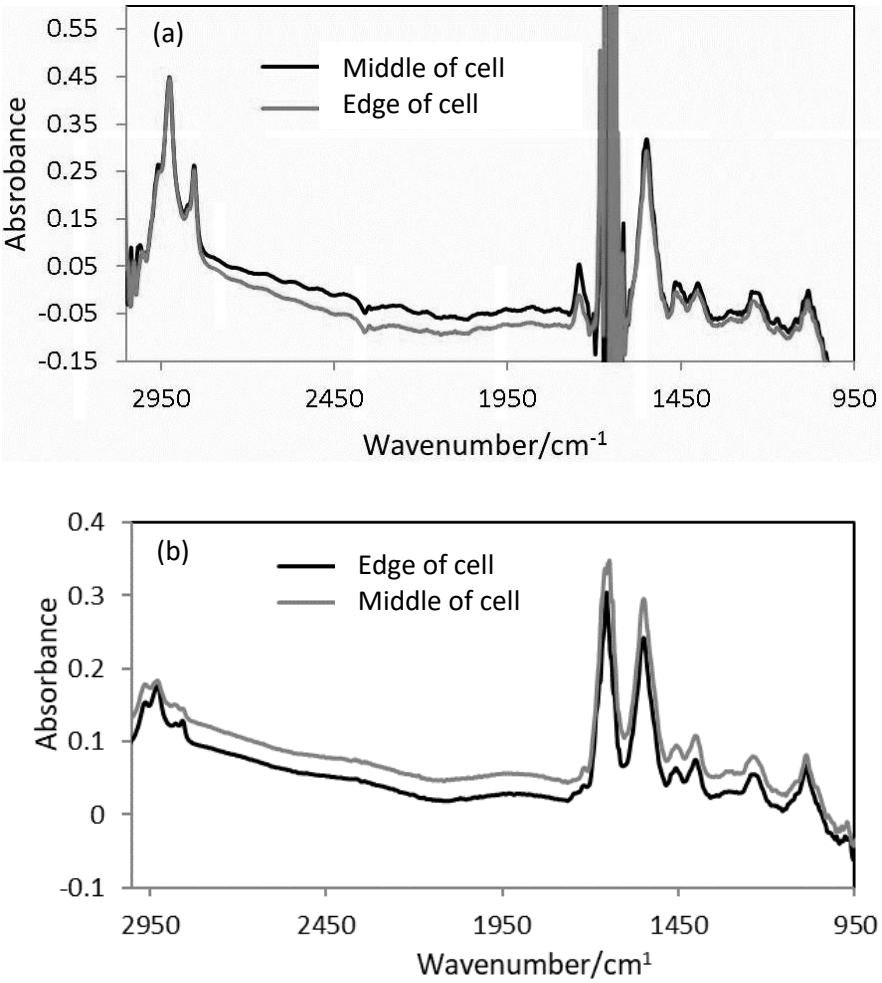

Figure S4: Synchrotron FTIR spectra (non-processed, non-averaged) measured through the ZnS hemispheres extracted from (a) the prototype device[1] (with less defined path length) and (b) the new device with controlled path length of 6 µm.

1. K. L. A. Chan, P. L. V. Fale, A. Atharawi, K. Wehbe, and G. Cinque, "Subcellular mapping of living cells via synchrotron microFTIR and ZnS hemispheres" Anal. Bioanal. Chem., 2018,410(25): 6477-6487